No Negative Radial Anisotropy below Cratons: Evidence from Bayesian Inversion

[1]Alistair Boyce, [1]Thomas Bodin, [1]Stephanie Durand, [1]Dorian Soergel

[1]Université Claude Bernard Lyon 1, ENS de Lyon, CNRS, UMR 5276 LGL-TPE, F-69622, Villeurbanne, France

1 Overview

• Global radial anisotropic models are inconsistent (Fig. 1) meaning geological interpretation of active/ancient mantle flow/deformation is challenging.

• One recent interpretation (Priestley et al., 2020) suggests that negative radial anisotropy in the CAM2016 model at ~150km depth within cratons reflects their formation by horizontal shortening/vertical thickening. This mechanism is not easily reconciled with other available models however.

• Using variable parameterizations within both LSQR and Bayesian inversions of Rayleigh and Love (R&L) surface wave dispersion curves, we test whether negative radial anisotropy is reliably recovered at upper mantle depths using synthetic models (Section 3) and whether anisotropic anomalies are required below cratons using real data inversions (Section 4).

• Both algorithmic and parameterization choices affect 'recovered' radial anisotropy meaning existing geological interpretations may be biased.

• Future work involves benchmark inversions for mid-ocean ridges & active mountain belts and a global inversion using the Bayesian algorithm (Soergel et al., in prep).

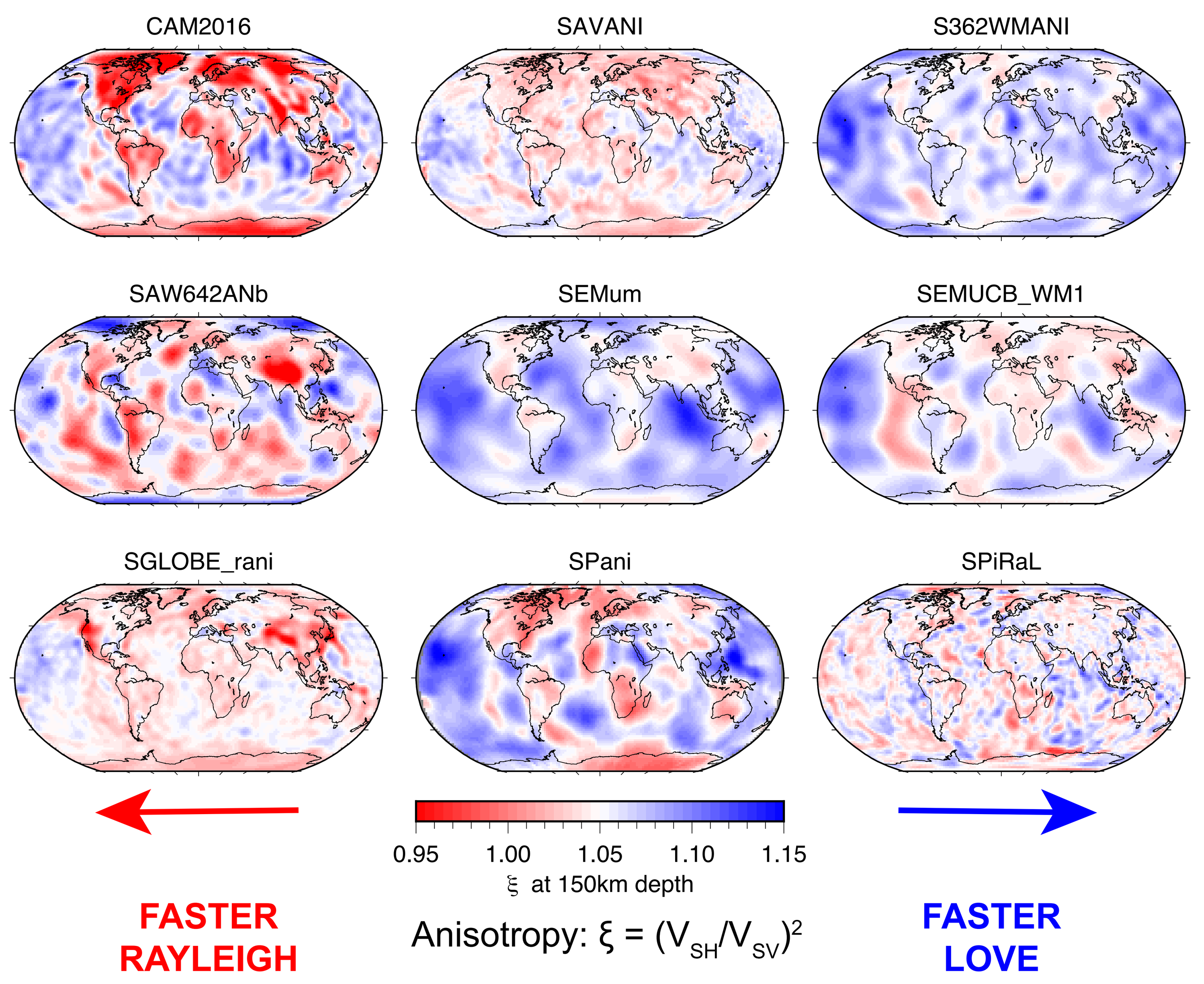

FIGURE 1: Nine published global radial anisotropy models (see references) at 150km depth plotted on a diverging color scale around Xi=1.05, the approximate Xi in PREM at 150km depth.

2 Methodologies

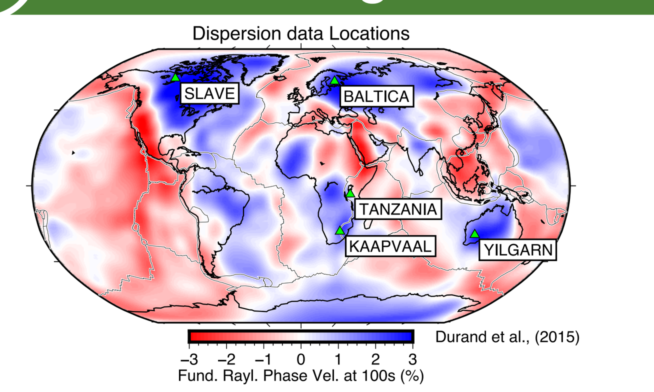

FIGURE 2: Fundamental mode Rayleigh wave phase velocity map at 100s period (Durand et al., 2015) w.r.t. mean value. Locations of data inversions in Section 4 are indicated.

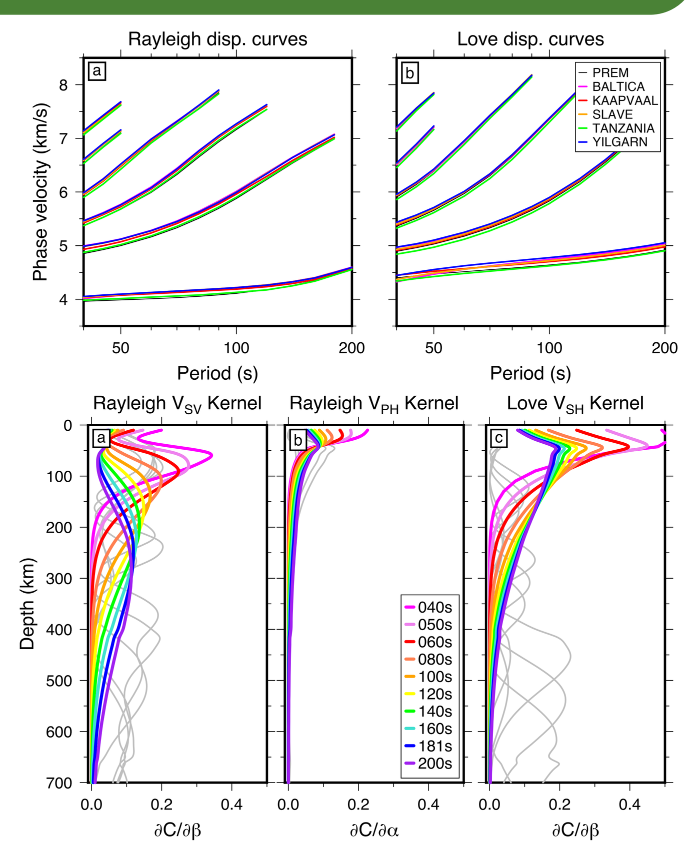

FIGURE 3 (upper): Rayleigh & Love (a,b) Fundamental mode and overtone (1-5) dispersion curve data extracted from phase velocity maps (Durand et al., 2015) at 40-200s period at 5 cratonic locations (see Figure 2) inverted in Section 4.
FIGURE 4 (lower): Fundamental mode (colored) and 3rd overtone (grey) sensitivity kernels for Rayleigh (V_{SV} & V_{PH}, a,b) and Love (V_{SH}, c) waves at a range of periods for modified PREM reference model.

• Reference model for all inversions: Modified PREM **without** 220km discont. & upper mantle radial ansiotropy.

• Sensitivity kernels (LSQR) & R&L dispersion curve forward modelling (Bayesian & synthetic models): **Mineos** (Masters et al., 2011).

• **2D LSQR inversion** based on Tarantola & Valette (1982) adapted from Debayle & Ricard (2012) used in Sections 3&4. Conservative regularisation parameters chosen on L-curve.

• **2D** hierarchical transdimensional **Bayesian inversion** using reversible jump Markov chain Monte Carlo sampling (adapted from Bodin et al., 2016) to 700km depth. Number of layers, presence/absence of anisotropy & data error are all free parameters. +/-40% prior used for V_{SV}, Xi & V_{PH}.

• **Fundamental & higher mode** (up to 5th overtone) **R&L dispersion curves** at **40-200s period** extracted from phase velocity maps (Durand et al., 2015) at 5 cratonic locations (Figs. 2&3) for inversion in Section 4.

• **For comparison:** V_{SV} & Xi profiles extracted from CAM2016 model (Priestley et al., 2020) at a range of horizontal smoothing length scales (Sections 3&4).

3 Synthetic Data Inversions

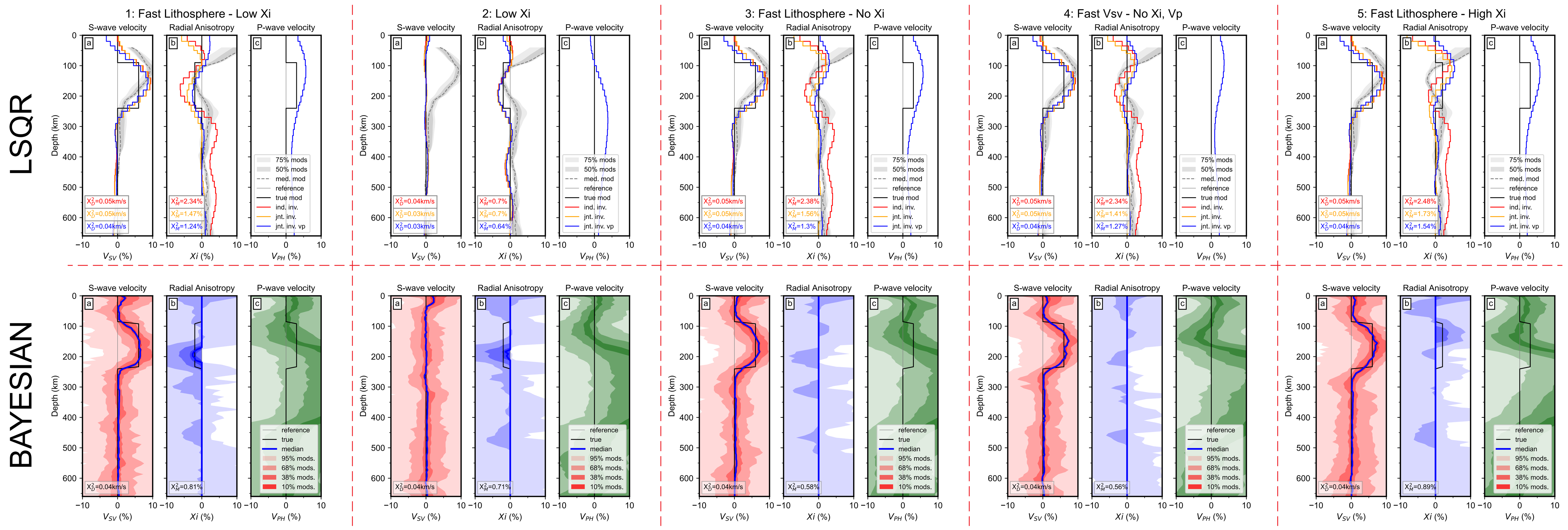

FIGURES 5-9 (Left): Five synthetic models inverted using variably parameterized LSQR algorithm. V_{SV}, Xi & V_{PH} shown in percent deviation from reference model (no anisotropy). Red curve: Independent inversion for V_{SV} & V_{SH}, Orange curve: Joint inversion for V_{SV} & V_{SH}, Blue curve: Joint inversion for V_{SV}, V_{SH} & V_{PH}. Chi squared data (X^2_D) and model (X^2_M for V_{SV} & Xi) fits are given. Grey line: Reference model, Black line: True model. Grey shaded regions and dashed curve (med. mod) show distribution of V_{SV} & Xi profiles from CAM2016 model (Priestley et al., 2020) extracted at cratonic locations (excluding Tanzania) explored in Section 5.

• LSQR: Independent inversions for V_{SV} & V_{SH} produce negative radial anisotropy at ~100-250km depth even for input models with positive or zero Xi anomalies. This issue is reduced in joint inversions.

• LSQR: Data & model fit improves with joint inversions, especially when V_{PH} is a free parameter.

• Bayesian: Similar data fit to LSQR, mostly improved model fit for synthetic inversions.

• Bayesian: Negative Xi artefacts not seen, although median model does not always recover Xi anomaly completely. True V_{PH} model frequently inside 1 S.D.

FIGURES 10-14 (Left): Five synthetic models inverted using Bayesian algorithm. Posterior distribution (credible intervals) of V_{SV}, V_{SH} & V_{PH} shown in percent deviation from reference model (no anisotropy). Blue curve: Median model. Chi squared data (X^2_D) and model (X^2_M for V_{SV} & Xi) fits are given. Grey line: Reference model, Black line: True model.

4 Real Data Inversions

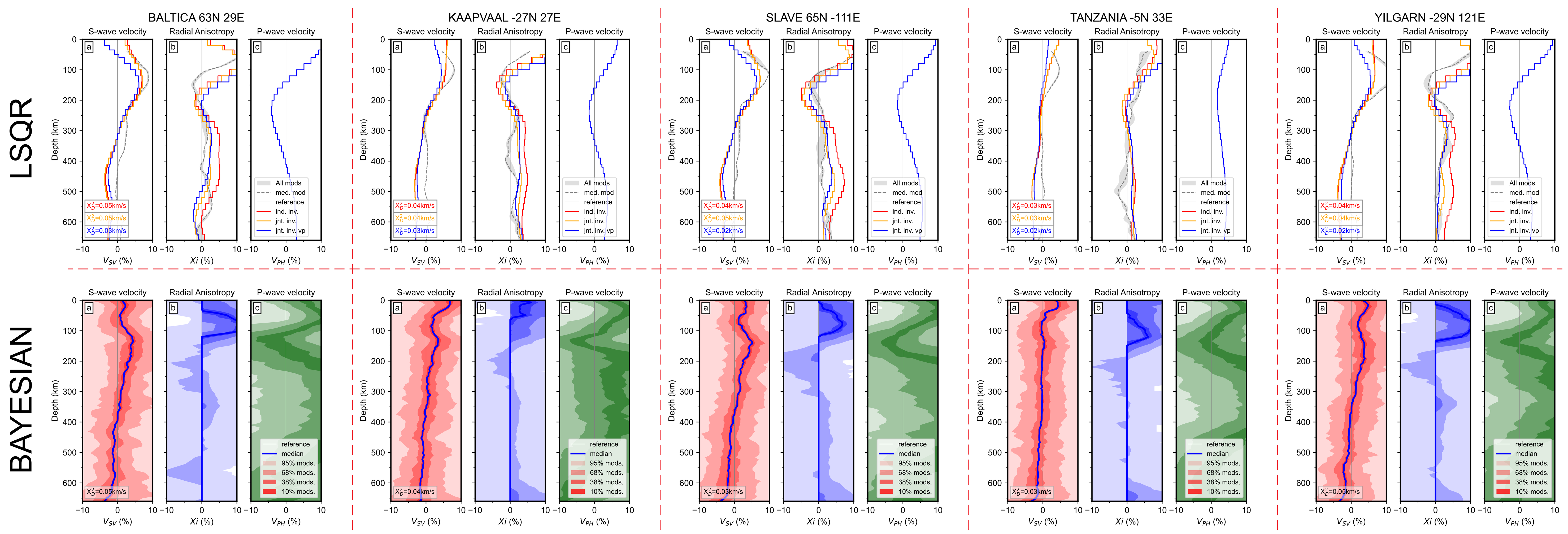

FIGURES 15-19 (Left): Five cratonic R&L dispersion curves (Fig. 3, Durand et al., 2015) inverted using variably parameterized LSQR algorithm. V_{SV}, Xi & V_{PH} shown in percent deviation from reference model (no anisotropy). Red curve: Independent inversion for V_{SV} & V_{SH}, Orange curve: Joint inversion for V_{SV} & V_{SH}, Blue curve: Joint inversion for V_{SV}, V_{SH} & V_{PH}. Chi squared data (X^2_D) fits are given. Grey line: Reference model, Grey shaded regions and dashed curve (med. mod) V_{SV} & Xi profiles from CAM2016 model (Priestley et al., 2020) extracted at each location.

• LSQR inversion results with variable parameterizations are well fit to CAM2016 V_{SV} & Xi profiles for 5 cratonic locations. Negative Xi at ~150-200km depth is reproduced most strongly with independent V_{SV} & V_{SH} inversion but is reduced using joint inversions especially with V_{PH} free (while data fit increases).

• Bayesian inversion with free V_{PH} parameterization shows no negative anisotropy below cratons. +5-10% Xi anomaly is pervasive at <150km depth in the mantle, similarly to PREM.

• Bayesian inversion of Tanzanian data shows atypical cratonic V_{SV} structure, but Xi structure is remarkably similar to other locations.

FIGURES 20-24 (Left): Five cratonic R&L dispersion curves (Fig. 3, Durand et al., 2015) inverted using Bayesian algorithm. Posterior distribution (credible intervals) of V_{SV}, Xi & V_{PH} shown in percent deviation (+/-10%) from reference model (no anisotropy). Blue curve: Median model. Chi squared data (X^2_D) fits are given. Grey line: Reference model.

5 Extreme Example with Synthetic Data

• Dispersion curves from synthetic input model (∂V_{PH}=-30%) inverted in Bayesian algorithm using fixed and free V_{PH} parameterizations.

• V_{PH} Fixed: Unconsidered V_{PH} variations cause V_{SV} & Xi artefacts in shallow mantle and transition zone (Fig. 25).

• V_{PH} Free: No artefacts in median V_{SV} & Xi models. Upper mantle V_{PH} variation well recovered, some artefacts at depth (Fig. 26).

• V_{PH} should be set free in inversions to reduce V_{SV} & Xi artefacts. V_{PH} anomalies may be recovered by fundamental and overtone dispersion data in some circumstances.

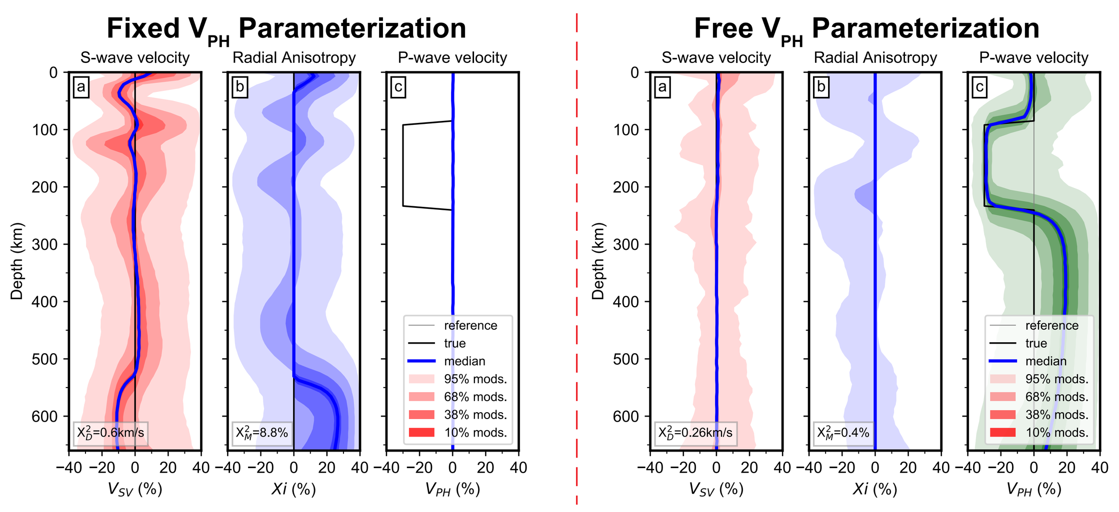

FIGURE 25 (Left): Synthetic model inverted using Bayesian algorithm with fixed V_{PH} parameterization. Posterior distribution (credible intervals) of V_{SV}, V_{SH} & V_{PH} shown in percent deviation (+/-40%) from reference model (no anisotropy). Blue curve: Median model. Chi squared data (X^2_D) and model (X^2_M for V_{SV} & Xi) fits are given. Grey line: Reference model.

FIGURE 26 (Right): Synthetic model inverted using Bayesian algorithm with free V_{PH} parameterization. Other lines/shades same as Fig. 25.

TAKE-HOME MESSAGES

1. **Negative radial anisotropy below cratons** (~150km depth) can be reproduced using classical LSQR inversion, but is **likely an artefact**…

2. **Bayesian inversion** with free V_{PH} parameterization yields **no negative radial anisotropy below cratons**, only +5-10% Xi above 150km depth similar to PREM.

3. **Craton formation by horizontal shortening** (Priestley et al., 2020) is **not favourable**.

4. **Set V_{PH} free** in surface wave inversions, preferably with Bayesian algorithms!

Funding statement:

This work received funding from the **European Research Council** (ERC) under the European Union's Horizon 2020 research and innovation programme (grant agreement No. 716542-TRANSCALE) and is supported by the **Centre National de la Recherche Scientifique** at unit UMR5276 (LGL-TPE).

References:

Bodin, T., et al., (**2016**) *Geophys J Int* doi: 10.1093/gji/ggw124. Debayle, E. & Ricard, Y. (**2012**) *J Geophys Res.* doi: 10.1029/2012jb009288. Durand, S., et al., (**2015**) *Geophys Res Lett.* doi: 10.1002/2015gl063700. Masters, G. et al., (**2011**), *Mineos v1.0.2, Computational Infrastructure for Geodynamics*, url: https://geodynamics.org/cig. Priestley, K. et al., (**2020**) *Geology*, doi: 10.1130/G47696.1. Tarantola, A. & Valette, B. (**1982**) *Rev Geophys.* doi: 10.1029/RG020i002p00219. ***Xi Models: CAM2016***: Priestley, K. et al., (**2020**) *Geology*, doi: 10.1130/G47696.1. ***SAVANI***: Porritt, R.W., et al., (**2021**) *Geophys. J. Int.* doi: 10.1093/gji/ggab185. ***S362WMANI***: Kustowski, B,G. et al., (**2008**), *J. Geophys. Res.*, doi: 10.1029/2007JB005169. ***SAW642ANb***: Panning, M.P., et al., (**2010**). *J. Geophys. Res.* doi: 10.1029/2010-JB007520. ***SEMum***: Lekic, V. & Romanowicz, B. (**2011**) *Geophys. J. Int.* doi: 10.1111/j.1365-246X.2011.04969.x. ***SEMUCB_WM1***: French, S.W. & Romanowicz, B. (***2014***) *Geophys. J. Int.* doi: 10.1093/gji/ggu334. ***SGLOBE-rani***: Chang, S.-J. et al., (**2015**) *J. Geophys. Res.*, doi: 10.1002/2014JB011824. ***SPani***: Tesoniero, A., et al., (**2015**), *J. Geophys. Res.* doi: 10.1002/2015JB012026. ***SPiRaL***: Simmons N.A., et al., (**2021**) *Geophys. J. Int.* doi: 10.1093/gji/ggab277.

alistair.boyce@univ-lyon1.fr / @alistair_boyce / alistairboyce11.github.io